Journal of Soft Computing and Information Technology (JSCIT)
Babol Noshirvani University of Technology, Babol, Iran
Journal Homepage: jscit.nit.ac.ir
Volume *, Number *, Spring 20**, pp. **-**
Received: **/**/**, Revised: **/**/**, Accepted: **/**/**

An Integrated Deep Learning Model for Wafer Defect Detection Using Joint Spatial and Temporal Feature Representation

Ali Souri[1], Samira Mavaddati[2]*, Mohammad Gholami[3]
1- Faculty of Engineering and Technology, University of Mazandaran, Babolsar, Iran.
2*- Associate Professor, Department of Electrical Engineering, Faculty of Engineering and Technology, University of Mazandaran, Babolsar, Iran.
3- Associate Professor, Department of Electrical Engineering, Faculty of Engineering and Technology, University of Mazandaran, Babolsar, Iran.
[1]a.souri09@umail.umz.ac.ir, [2*]s.mavaddati@umz.ac.ir, and [3]m.gholami@umz.ac.ir

Corresponding author's address: Samira Mavaddati, Department of Electrical Engineering, Faculty of Engineering and Technology, University of Mazandaran, Babolsar, Iran.

Abstract- Wafer defect detection is vital in semiconductor manufacturing due to its impact on the reliability and performance of integrated circuits. Defects such as microcracks, contamination, and pattern misalignment can cause device failures. In this study, we propose an improved hybrid deep learning framework that integrates Convolutional Neural Networks (CNN) for extracting spatial features with Long Short-Term Memory (LSTM) networks to model temporal dependencies in defect patterns. By combining both spatial and sequential information, the method enhances the accuracy of defect classification compared to conventional approaches. Evaluations on MIR-WM811K and WaferMap datasets show superior performance, achieving accuracies of 98.12% and 97.38%, respectively. The proposed CNN-LSTM model outperforms existing architectures, including RCNN, VGG-16, ResNet-34, and DenseNet-121. Its strength lies in the integrated spatial–temporal learning, which captures complex defect characteristics more effectively. This method sets a new baseline for deep learning–based wafer inspection, with strong potential to enhance manufacturing efficiency and product quality in the semiconductor industry.

Keywords- Wafer defect detection, Spatial and temporal feature, Deep learning, Semiconductor industry.

I. INTRODUCTION

The semiconductor sector forms the foundation of contemporary technology, enabling advancements across consumer electronics, automotive applications, telecommunications, and healthcare devices. Central to this industry are wafers, thin slices of semiconductor material that serve as the substrate for integrated circuits (ICs). Ensuring the quality of these wafers is critical, as defects such as scratches, contamination, or microcracks can compromise electronic components' performance, reliability, and lifespan [1-2]. Traditionally, wafer defect detection has relied on manual inspection or conventional machine vision techniques. While these methods have been effective to some extent, they face significant limitations regarding scalability, consistency, and sensitivity to subtle defect patterns. Over the years, machine learning methods have been explored to overcome these challenges. Machine learning methods like Support Vector Machines (SVMs), Random Forests, and K-Nearest Neighbors (K-NN) have demonstrated potential for automating defect detection by identifying patterns from annotated datasets [3]. Nevertheless, these approaches typically demand substantial feature engineering and often struggle to generalize across varied defect categories and operating conditions.

In contrast, deep learning models have revolutionized the field of defect detection by automating feature extraction and learning hierarchical representations directly from raw data [4-5]. Convolutional Neural Network (CNNs) have proven highly effective for handling image data, making them particularly suitable for detecting spatial patterns in wafer defects.

Despite their success, CNNs are inherently limited in capturing temporal or sequential dependencies, which may be crucial in analyzing patterns across a series of images or data points. To overcome this shortcoming, we introduce a hybrid CNN-Long Short-Term Memory (CNN-LSTM) framework that combines the spatial feature extraction power of CNNs with the sequential modeling capabilities of

LSTM networks. By combining these two architectures, the model can exploit both spatial and temporal features, improving its accuracy and reliability in detecting and classifying wafer defects. This choice is motivated by the complementary strengths of CNNs and LSTMs: while CNNs excel at capturing localized spatial features, LSTMs effectively model long-term dependencies and temporal sequences. This study concentrates solely on deep learning approaches due to their superior scalability and performance compared to conventional machine learning techniques. The proposed hybrid CNN-LSTM model is benchmarked against leading deep learning architectures, highlighting its effectiveness as a reliable method for automated wafer defect detection.

The structure of the paper is as follows: Section 2 reviews existing literature on both traditional and deep learning methods for defect identification. Section 3 describes the design and methodology of the CNN-LSTM framework. Section 4 reports experimental findings and compares the results with baseline models. Finally, Section 5 provides conclusions and discusses potential avenues for future research.

II. RELATED WORK

Ensuring high-quality wafer production while reducing manufacturing costs has made defect detection a crucial research focus in the semiconductor industry. Over time, numerous methods have been developed to automate this process, ranging from conventional image processing techniques to sophisticated machine learning and deep learning approaches. Initial wafer inspection systems mainly relied on rule-based image analysis, employing methods such as edge detection, morphological transformations, and template matching. While these methods were effective for simple defect patterns, their performance significantly degraded when faced with complex or subtle defects, often requiring manual tuning and expert knowledge. To overcome these limitations, machine learning algorithms were introduced, enabling systems to learn defect patterns from labeled datasets. Methods such as SVMs, Decision Trees, and Random Forests achieved notable success by leveraging handcrafted features, including texture descriptors and statistical measures. Nevertheless, these early approaches depended heavily on manual feature engineering, which restricted their flexibility in handling diverse defect types and varying operational conditions. The introduction of deep learning transformed defect detection, with CNNs becoming the preferred method due to their capacity to automatically learn hierarchical feature representations from raw images, markedly surpassing the performance of traditional techniques. Models like Visual Geometry Group 16 (VGG16), Residual Network (ResNet), and MobileNet have been widely used in wafer defect detection, demonstrating remarkable accuracy and robustness. Despite their strengths in capturing spatial features, CNNs alone often struggle with modeling sequential or temporal dependencies, which can be essential in certain defect detection tasks.

Using advanced deep learning techniques, this paper examines the capabilities of deep models and the outcomes obtained in solving the wafer defect detection problem, highlighting their impact on the electronics and semiconductor industries. For instance, in [6], a novel approach for the automatic classification of defects in semiconductor wafers using deep learning is proposed. This method employs a CNN to extract effective features from Scanning Electron Microscope (SEM) images, followed by a K-NN algorithm for defect classification. This approach significantly improves classification performance compared to traditional methods and can identify unseen defects during training. In [7], two approaches for utilizing deep CNNs for defect classification were proposed: training a CNN with five convolutional layers and employing a pre-trained Recurrent Convolutional Neural Network (RCNN) with transfer learning. A novel labeling-rule-based method, presented in [8], is insensitive to pattern rotations and inversions. This model uses the Radon transform and kernel inversion to achieve geometric invariance. The study in [9] investigated computer vision-based approaches for the automated classification of wafer defects. A classifier capable of identifying type A and B defects on wafers was proposed, built on a five-layer CNN, and trained with 250 images per class from the wafer map dataset. According to [10], precise detection and classification of wafer defects are crucial components in semiconductor manufacturing. Such information provides interpretable insights into potential defect causes, facilitating corrective measures and quality improvement. An enhanced You Only Look Once (YOLO) framework was introduced in this study to achieve precise localization and classification of wafer defects. In [11], deep learning algorithms, such as CNNs, were applied to classify wafer defects in the semiconductor industry. A two-stage strategy integrating conventional computer vision methods with a compact SqueezeNet model was proposed and evaluated against more complex CNN architectures.

In [12], a novel technique was introduced to represent defect patterns as low-dimensional vectors, which are subsequently fed into a neural network for classification. The approach relies on extracting topological characteristics of each defect using persistent homology from Topological Data Analysis (TDA). Experiments conducted on simulated datasets showed that this method surpassed CNN-based approaches in both accuracy and computational efficiency. As reported in [13], Automated Defect Classification (ADC) remains a widely adopted method in semiconductor manufacturing, leveraging optical or Scanning Electron Microscopy (SEM) images for defect identification. In [14], a deep selective learning framework for wafer map defect classification was proposed, incorporating a rejection mechanism to avoid class predictions when the risk of misclassification is high, thereby balancing coverage and error. To enhance defect detection precision and optimize yield, [15] introduced a Multi-Feature Fusion Perceptual Network (MFFP-Net) inspired by human visual perception, which processes and integrates features across multiple scales. Additionally, [16] addressed the challenges of wafer map defect classification under imbalanced sample distributions. A model leveraging de-noising and probabilistic diffraction with an auxiliary classifier was proposed to generate new wafer maps. The model employs a U-Net structure with multiple inputs and outputs, using wafer images, noise levels, and classification features as

inputs, and predicting noise and classifications as outputs. In [17], an anomaly-driven generative adversarial network (GAN) framework was employed to address the problem of data imbalance in wafer defect classification. The framework integrates a Variational Autoencoder-GAN (VAE-GAN) to generate additional samples alongside a classifier for wafer defects.

VAE-GAN integrates the benefits of probabilistic autoencoders (VAE) and GANs to create realistic new images while avoiding ambiguous or unreasonable outputs. In [18], the goal was to classify wafer map defect patterns with minimal resources and time. An efficient CNN model focusing on advanced performance, resource efficiency, and fast processing time was explored for this purpose.

Recent research has explored hybrid architectures to address these limitations, combining CNNs with sequential models such as Recurrent Neural Networks (RNNs) and their variants, LSTM networks. These hybrid models leverage the complementary strengths of CNNs and LSTMs, capturing both spatial and temporal features to enhance defect detection performance. However, there remains room for improvement in balancing model complexity and computational efficiency while maintaining high accuracy. This paper builds upon these advancements by proposing a CNN-LSTM hybrid framework tailored for wafer defect detection, aiming to address the limitations of existing methods and further enhance detection accuracy and reliability. The main contributions of this article are as follows:

- Introduction of a hybrid CNN-LSTM model for wafer defect detection: This study proposes a novel hybrid deep learning model that integrates CNN for spatial feature extraction and LSTM networks for capturing temporal dependencies in wafer defect data. This hybrid architecture enhances the model's ability to understand both spatial and sequential patterns, which is critical for detecting defects that occur in sequences or have spatial relationships.
- Comprehensive evaluation of the CNN-LSTM framework: The proposed CNN-LSTM model is rigorously evaluated on a benchmark wafer defect dataset, demonstrating its ability to outperform traditional CNN-based approaches regarding classification accuracy. The framework leverages both spatial and temporal features to capture the complexity of wafer defects better, leading to improved performance.
- Comparative analysis with state-of-the-art architectures: This paper compares the performance of the CNN-LSTM hybrid model with other popular deep learning architectures, such as CNN, Recurrent Convolutional Neural Networks (RCNN), VGG16, ResNet34, and DenseNet121. The results highlight the superior accuracy and robustness of the CNN-LSTM model, showcasing its potential for real-world applications in automated wafer defect detection.
- Significant improvement in classification accuracy: This paper demonstrates a substantial increase in classification accuracy with the CNN-LSTM framework, making it a more effective tool for defect detection in semiconductor manufacturing in comparison to standalone CNN models. This improvement is crucial for enhancing automated quality control processes.
- Implications for semiconductor industry applications: The proposed method offers significant advantages for the semiconductor industry, particularly in enhancing the efficiency and accuracy of wafer defect detection systems. The ability to learn both spatial and temporal features positions the CNN-LSTM model as a promising solution for high-precision quality control in semiconductor manufacturing.
- Advancement in automated quality control: The paper emphasizes the role of hybrid deep learning models in advancing automated quality control systems, providing a more reliable and efficient approach to detecting wafer defects. This work lays the foundation for further exploration and development of defect detection technologies in the semiconductor industry.

These contributions provide valuable insights into the application of hybrid deep learning models for defect detection, with the potential to drive innovation in automated quality control processes within the semiconductor manufacturing sector.

Table I presents recent studies based on deep learning concepts for wafer defect detection in semiconductor manufacturing processes. This Table provides a comprehensive comparison of the proposed methods, research objectives, data sources, the number of categories used in classification, and the publication years of each study.

III. PROPOSED METHODOLOGY

This section describes the methodology of the proposed hybrid deep learning model for detecting wafer defects in semiconductor manufacturing. The approach integrates a CNN for extracting spatial features and an LSTM network for capturing temporal dependencies within defect data. The methodology is organized into several components: dataset preparation and augmentation, the CNN architecture for spatial feature extraction, the LSTM architecture for temporal modeling, model configurations and hyperparameters, and evaluation metrics. In the subsections that follow, each component of the proposed framework is presented and discussed in detail.

A. Dataset Description and Augmentation

This study utilizes a publicly accessible wafer defect dataset containing multiple defect categories, including microcracks and contamination [19, 20].

In this paper, the classification of eight common wafer defect severity classes is evaluated, which include the following:

- Center Defect: This class refers to defects that appear in the center of the wafer. These defects may arise from contamination, bubbles, or other issues during the early stages of the manufacturing process [21].

TABLE I
RECENT STUDIES ON WAFER DEFECT DETECTION IN INTEGRATED CIRCUITS BASED ON DEEP LEARNING MODELS

Reference	Task	Classes	Dataset	Classifier	Year
[6]	Detection/ Classification	5 Classes (Spot, Rock-shaped particle, Ring-shaped particle, Misalignment, Scratch)	DatasetTT/ Dataset-UN	CNN	2019
[7]	Classification	4 Classes (Scrap, Random, Local, Center)	COCO/ KITTI	CNN	2020
[8]	Classification	7 Classes (Center, Donut, Edge-loc, Edge-Ring, Loc, Random, Scratch)	WM-811K wafer Defect	CNN	2023
[9]	Classification	2 Classes (Random, Edge-Ring)	WBM dataset	CNN	2022
[10]	Detection/ Classification	9 Classes (Center, Donut, Edge-loc, Edge-Ring, Loc, Random, Scratch, Near-full, None)	WM-811K wafer Defect	YOLOv3/YOLOv4	2022
[11]	Detection/ Classification	8 Classes (NO Defect, Class A, Class B, Class C, Class D, Class E, Class F, Class G)	Surface Defect Dataset	SqueezeNet CNN	2023
[12]	Classification	5 Classes (Random, Ring, Scratch, Dense, Cluster)	WM-811K	CNN	2023
[13]	Classification	12 Classes (Defocus, ICP, Broken, OX residue, Partial etch, Poly bump, Poly residue, PR damage, PR residue, Scratch, Silicon, Surface particle)	-	DNN	2022
[14]	Classification	9 Classes (Center, Donut, Edge-loc, Edge-Ring, Loc, Random, Scratch, Near-full, None)	WM-811K wafer Defect	CNN	2020
[15]	Classification	8 Classes (Center, Donut, Edge-loc, Edge-Ring, Loc, Random, Scratch, Near-full)	WM-811K/ WaferMap	MFFP-Net	2023
[16]	Classification	9 Classes (MIR-M811K)/ 28 Classes (MixedWM38)	MIR-M811K /MixedWM38	ResNet	2024
[17]	Classification	8 Classes (Center, Donut, Edge-loc, Edge-Ring, Loc, Random, Scratch, Near-full)	WM-811K wafer Defect	VAE-GAN	2022
Proposed CNN/LSTM-Based Method	Classification	9 Classes (Center, Donut, Edge-loc, Edge-Ring, Loc, Random, Scratch, Near-full, None)	WM-811K wafer Defect	RCNN/VGG16/ ResNet34, DenseNet121 /CNN-LSTM	-

- Donut Defect: This class includes defects that resemble a donut shape, with a dark center and brighter edges. These defects are often caused by issues related to photolithography or etching processes.
- Edge-local Defect: This class includes defects located at the edges of the wafer, particularly near where the components are placed. These defects can result from mechanical damage or packaging-related issues.
- Edge-ring Defect: This class encompasses defects that appear ring-like at the edges of the wafer. These defects are commonly caused by issues related to the chemical vapor deposition (CVD) process.
- Local Defect: This class refers to defects that appear at specific locations on the wafer, such as where gates or connections are placed. These defects may stem from design flaws or process-related problems.
- Random Defect: This class includes defects that are randomly distributed across the wafer surface. These defects may be due to contamination, dust, or other environmental factors.
- Scratch Defect: This class refers to scratches on the wafer surface. These scratches can result from mechanical damage, improper cleaning, or handling issues.
- Nearly Complete Defect: This class includes defects that almost cover the entire surface of the wafer. These defects are often caused by issues in the etching or cleaning processes [22].

A key limitation of this study is the availability of publicly accessible wafer defect datasets, as our experiments were primarily conducted on MIR-WM811K and WaferMap, limiting the diversity of data and potentially affecting the generalizability of the proposed model. Figure 1 illustrates sample images of each defect class on the wafer surface. In addition to these primary defect classes, sub-classes may also be used for more precise defect classification. One of the comprehensive datasets widely used in wafer defect detection studies is the MIR-WM811K dataset. This publicly available dataset is used for wafer defect classification in the semiconductor industry [19]. Maintained by the MIR Lab at Seoul National University, this dataset is freely accessible on the Pattern Recognition Lab website and has been used by researchers worldwide, enabling the comparison of results obtained with this dataset [19]. The dataset consists of 811,457 wafer maps collected across 46,393 categories from real production processes, offering extensive information to support deep learning-based defect detection. For comparative evaluation of the proposed model against others, the WaferMap dataset, which includes nine distinct classes, was also employed.

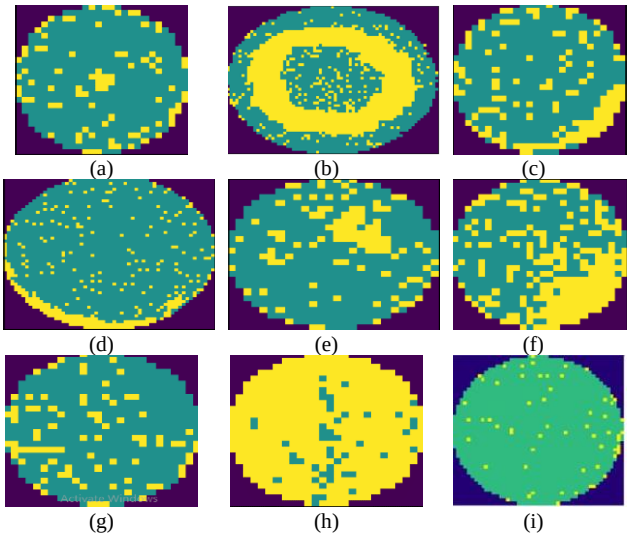

Fig. 1. A sample of wafer defect images in the classes of: a) Center, b) Donut, c) Edge-local, d) Edge-ring, e) Local, f) Random, g) Scratch, and h) Near-full, and i) None.

Table II presents the number of images in each defect category before and after applying data augmentation techniques [20]. In this study, deep learning models are utilized for wafer defect detection in integrated circuits, where high precision is essential. Models such as CNN, RCNN, VGG16, and DenseNet121 are employed due to their capability to extract complex features and identify intricate patterns in images. A major challenge in wafer defect detection is the imbalance or scarcity of samples for certain defect types, which can negatively affect the stability and accuracy of deep learning models. To enhance generalization and robustness, data augmentation techniques, such as rotation, flipping, scaling, cropping, brightness adjustment, and reflection, are applied to increase the diversity of training samples [23-25]. These transformations allow the models to learn more complex features, improve recognition of rare patterns, and mitigate overfitting by preventing the model from focusing solely on specific details of limited samples. As a result, the augmented data helps the model acquire more stable and generalizable feature representations, leading to improved performance on unseen data.

It should be noted that the applied augmentation techniques, such as small rotations (±10°), flipping, resizing, translation, and minor brightness adjustments, are designed to preserve the inherent characteristics of wafer defect patterns. Since wafer maps are approximately circular and rotationally symmetric, these transformations do not distort the spatial relationships between dies. Augmented data images for eight defect categories from the dataset are shown in Figure 2.

Augmentation techniques, such as rotation, resizing, translation, and brightness adjustment, help increase data diversity and prevent overfitting. The increased number of images per category improves the model's ability to generalize to new data, enhancing defect detection accuracy. Another powerful strategy for enhancing deep learning model performance is transfer learning.

It allows models to use knowledge gained from one domain to address a new task. To illustrate the impact of data augmentation on the training dataset, Figure 3 presents the distribution of wafer defect categories before and after applying augmentation techniques. The dataset is derived from the MIR-WM811K wafer defect. In wafer defect detection, due to limited training data, leveraging pre-trained models on larger, general datasets can significantly improve accuracy and performance. Transfer learning involves first training models on larger datasets like ImageNet and then fine-tuning them on wafer-specific defect data [26-28].

This process allows the model to benefit from general knowledge of complex patterns and then focus on learning specific defect patterns. Transfer learning reduces the need for large datasets in the second phase and can yield significant results even with limited data. Another advantage of transfer learning is reduced training time [29]. Since the model has already been trained on a large dataset, there is no need for long training on wafer data, making it especially effective in industrial environments where speed and precision are critical [30].

TABLE II
THE NUMBER OF IMAGES FOR EACH WAFER DEFECT CATEGORY BEFORE AND AFTER DATA AUGMENTATION TECHNIQUES FROM THE MIR-WM811K DATASET

Defects	Total Data	Train Data	Test Data	After Augmentation (Train Data)
Center	2160	1512	648	7560
Donut	2002	1400	602	7000
Edge-Loc	2368	1657	711	8285
Edge-Ring	2046	1432	614	7160
Loc	2376	1663	713	8315
Random	2146	1502	644	7510
Scratch	2088	1461	627	7305
Near-Full	2032	1422	610	7110
None	2489	1742	747	8710
Total	**19707**	**12441**	**5916**	**62511**

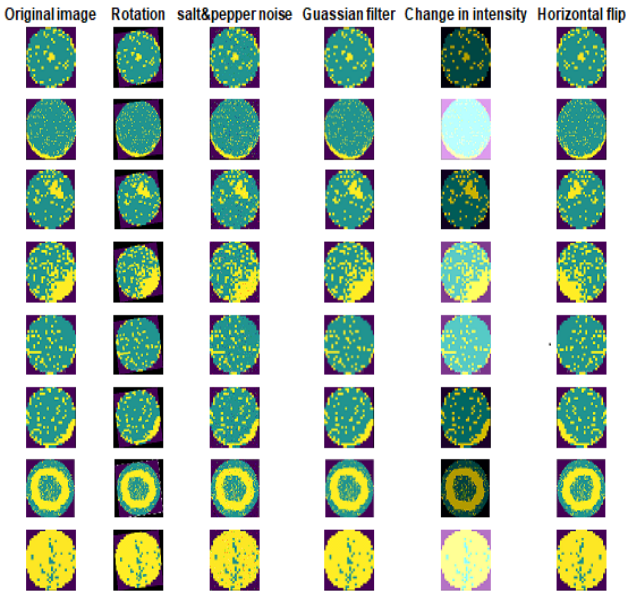

Fig. 2. A sample of augmented data images, including defect classes in each row from the MIR-WM811K dataset.

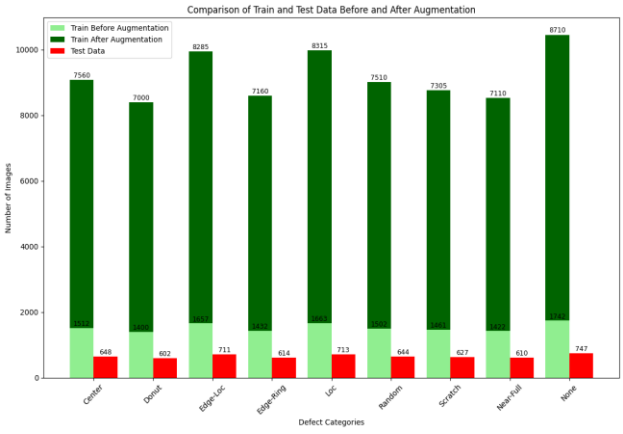

Fig. 3. Distribution of wafer defect classes prior to and following the application of data augmentation techniques. The bar chart shows the number of training and testing images for each defect category from the MIR-WM811K dataset. The green shades represent the training data before and after augmentation, while the red shade represents the testing data. The total dataset size increases significantly after augmentation, enhancing the training process for deep learning models.

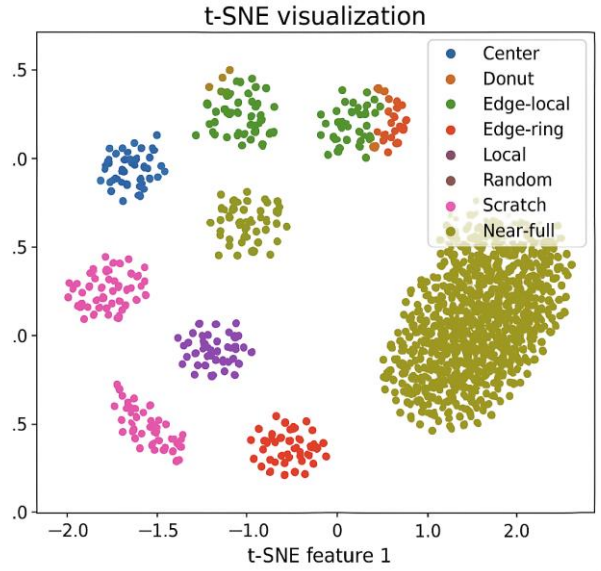

Fig. 4. The t-SNE visualization of original and augmented data features.

Figure 4 illustrates the t-SNE visualization of the features extracted from both the original and augmented datasets. This Figure provides a two-dimensional representation of the high-dimensional feature space, allowing us to observe how the augmentation process affects the distribution of data points. As shown, the augmented data expands the feature space and enhances the diversity of the samples, which can help improve the robustness and generalization of the model.

B. Convolutional neural network design for spatial feature extraction

The CNN module in the proposed framework is responsible for extracting spatial features from wafer defect images. It comprises several convolutional layers with diverse filter sizes, followed by ReLU activation functions and pooling layers to downsample the feature maps. This structure enables the network to capture significant spatial patterns associated with defects. The CNN component of the proposed model serves as a fundamental building block for extracting spatial features from wafer defect images. This architecture is designed to capture intricate patterns and localized details that are essential for accurate defect classification. It begins with multiple convolutional layers that apply filters of varying sizes, such as 3×3 and 5×5, to the input images. These filters are responsible for identifying both fine-grained and broader structural patterns within the defect regions. By sliding across the image and performing element-wise operations, these layers generate feature maps that emphasize critical spatial characteristics like edges, textures, and defect contours.

To improve the network's ability to learn more abstract and complex features, the Rectified Linear Unit (ReLU) is incorporated after each convolution step. By adding this non-linear mapping, the model becomes capable of representing non-linear dependencies in the input data. Subsequently, pooling operations, most commonly max-pooling, are utilized to shrink the spatial size of the generated feature maps. Through this process, the network retains the most significant characteristics while lowering sensitivity to spatial variations, leading to higher computational efficiency with minimal impact on classification accuracy.

To ensure the robustness of the model, additional techniques like dropout and batch normalization are incorporated. During the training phase, dropout layers temporarily deactivate a subset of neurons at random, which helps to limit overfitting and strengthens the model's ability to generalize. In contrast, batch normalization adjusts and standardizes the intermediate activations, allowing the network to converge more quickly and operate more stably.

In the concluding phase of convolution, a fully connected layer compiles the spatially extracted features into a dense, high-dimensional vector. This vector is then passed to the LSTM unit, which is designed to model temporal dependencies. The overall framework is optimized to tackle the difficulties inherent in wafer defect identification.

Its ability to handle high-resolution images ensures that even subtle defects, such as microcracks or contamination, are accurately identified. Additionally, the multi-scale feature extraction capability of the CNN allows it to adapt to the diverse types of defects commonly encountered in wafer manufacturing. By balancing computational efficiency with the complexity of the task, this CNN design establishes a robust foundation for the hybrid CNN-LSTM framework, significantly contributing to the overall accuracy and reliability of the defect detection process. In summary, CNN architecture plays a pivotal role in learning meaningful spatial features, effectively bridging the gap between raw image data and high-level defect classification. Through its hierarchical design and integration of advanced techniques, it ensures precise and efficient spatial feature extraction, paving the way for enhanced performance in automated wafer defect detection.

C. LSTM architecture for temporal dependency processing

To address the sequential nature of defect occurrence during wafer production, the LSTM network is employed as a critical component of the proposed model. LSTM networks are engineered to model temporal dependencies by retaining information over long sequences, making them well-suited for analyzing patterns and trends across multiple stages of the manufacturing process [31-33]. The LSTM architecture includes memory cells along with input, forget, and output gates, which control information flow. These gates allow the network to selectively preserve relevant temporal features while discarding irrelevant or noisy data at each timestep. This capability allows the LSTM to model the progression of wafer defects, which may depend on earlier stages of the production process or cumulative effects from preceding steps. The input to the LSTM component is the high-dimensional spatial feature representation generated by the CNN, which is transformed into a sequential format. The LSTM processes this sequential data, learning long-term dependencies and contextual relationships between features. For example, the presence of certain patterns in early-stage images may correlate with specific defect types observed in later stages. By capturing such temporal relationships, the LSTM contributes to a more

holistic understanding of the defect data. The LSTM output is typically passed through fully connected layers or a softmax classifier to produce the final predictions. This ensures that the temporal features extracted by the LSTM are effectively utilized for accurate classification. Furthermore, dropout is incorporated within the LSTM layers to mitigate overfitting, while techniques like gradient clipping are applied during training to stabilize the learning process. This design enables the model to recognize sequential trends, such as recurring defect patterns or the progression of contamination across manufacturing stages. Incorporating temporal context within the framework, the LSTM structure improves the model's capacity to more accurately differentiate among various defect categories. Overall, the incorporation of LSTM networks bridges the gap between spatial and temporal domains, allowing the hybrid CNN-LSTM model to learn comprehensive representations of wafer defects. This integration not only improves classification accuracy but also demonstrates the potential of leveraging temporal dependencies for advancing automated quality control in semiconductor manufacturing.

Although wafer defect datasets are primarily represented as two-dimensional wafer maps, the spatial arrangement of dies inherently introduces sequential dependencies. Defect propagation is rarely random; instead, it often follows progressive patterns across neighboring regions of the wafer. For instance, contamination or misalignment may start locally and gradually spread across adjacent dies. Such progression can be modeled as a sequence of states, where the order of defect appearances resembles temporal relationships [2, 14, 27]. Therefore, incorporating LSTM enables our model to capture these sequential dependencies, complementing CNN's spatial feature extraction and leading to a more comprehensive defect representation.

D. Model settings and hyperparameters

The configuration of the hybrid CNN-LSTM model involves carefully selected hyperparameters, tailored to maximize performance and ensure robustness in wafer defect detection. The CNN and LSTM modules have been individually designed and fine-tuned to work in harmony, forming a hybrid architecture that efficiently captures both spatial and temporal features. In the CNN segment, convolutional layers employ a mix of 3×3 and 5×5 kernels to extract features at different scales. These filter sizes allow the network to capture both fine details and broader patterns within the defect images. Batch normalization is incorporated after each convolutional layer to stabilize training by normalizing intermediate activations, which accelerates convergence and enhances generalization. Dropout layers with a rate of 0.5 are employed to prevent overfitting by randomly disabling a subset of neurons during training. Pooling layers are used to reduce the spatial dimensions of feature maps, maintaining a balance between computational efficiency and the retention of important spatial information. For the LSTM component, the architecture incorporates multiple hidden units, with the exact number determined through experimentation to balance complexity and performance. Each LSTM hidden unit sequentially processes input data across multiple timesteps, allowing the network to capture long-term dependencies and temporal patterns in wafer defect data. To improve generalization and prevent overfitting, a dropout rate of 0.2 is applied within the LSTM layers. The hybrid CNN-LSTM model is trained using the Adam optimizer, selected for its efficiency and adaptive learning capabilities, with an initial learning rate of 0.001 to ensure stable convergence. An adaptive learning rate scheduler further adjusts the rate when validation performance plateaus, enhancing the optimization process. Categorical cross-entropy is employed as the loss function, suitable for multi-class classification tasks. Training is conducted in batches of 32, striking a balance between computational efficiency and convergence stability. Early stopping monitors validation loss to halt training once improvements cease, mitigating overfitting. Model performance is assessed through multiple metrics, including accuracy, precision, recall, and F1-score, offering a comprehensive evaluation of defect detection capabilities. This carefully configured setup of hyperparameters and training strategies ensures the hybrid CNN-LSTM model effectively captures both spatial and temporal information, achieving high reliability and accuracy in classifying wafer defects.

Table III provides an overview of the main settings and hyperparameters adopted in the proposed CNN-LSTM hybrid framework. The configuration covers design elements such as convolutional kernel dimensions, dropout probabilities, and pooling mechanisms within the CNN, along with the number of hidden nodes and time-related parameters in the LSTM. Furthermore, Table III lists the training details, including the optimizer, learning rate, and batch size, as well as the evaluation criteria used to measure performance. Such a detailed setup is essential for achieving reliable and precise wafer defect detection.

TABLE III
OVERVIEW OF THE HYBRID CNN-LSTM MODEL: ARCHITECTURAL SETTINGS, TRAINING PARAMETERS, AND PERFORMANCE METRICS

Parameter	Component	Value/Setting	Description
Filter sizes	CNN	3×3, 5×5	Enable extraction of both local details and broader spatial patterns.
Batch normalization	CNN	After each convolution	Improves stability of training and supports faster convergence.
Dropout rate	CNN	0.5	Mitigates overfitting by randomly disabling neurons during learning.
Pooling type	CNN	Max-pooling	Shrinks feature maps while preserving key information.
Hidden units	LSTM	128	Defines the network's ability to represent sequential dependencies.
Dropout rate	LSTM	0.2	Promotes better generalization in sequence modeling.
Optimizer	Model-wide	Adam	Provides adaptive step sizes for efficient parameter updates.
Learning rate	Model-wide	0.001	Maintains stable and consistent progress during optimization.
Batch size	Model-wide	32	Specifies the number of samples handled per training step.
Loss function	Model-wide	Categorical cross-entropy	Appropriate for tasks involving multiple classes.
Early stopping	Training phase	Enabled	Stops training once validation loss ceases to improve.
Evaluation metrics	Testing phase	Accuracy, Precision, Recall, F1-score	Offer a complete assessment of classification quality.

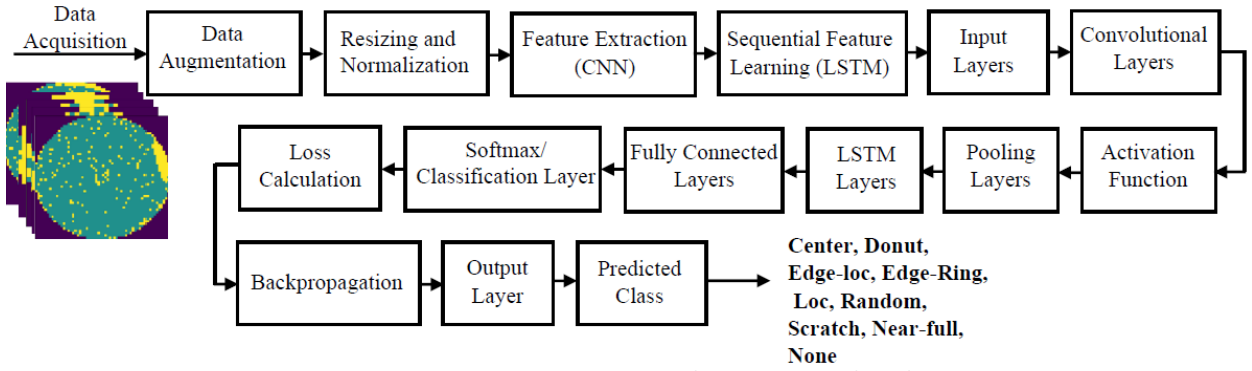

Fig. 5. Block diagram related to the designed CNN-LSTM combination model for automated wafer defect detection. The diagram illustrates the entire process from data acquisition and preprocessing to the feature extraction using CNN for spatial features, followed by sequential learning with LSTM to capture temporal dependencies. The model is then evaluated through classification layers and performance metrics, providing a comprehensive overview of the hybrid architecture designed for enhanced defect detection accuracy.

Algorithm 1: Pseudo-code for Wafer Defect Classification Using a Hybrid CNN-LSTM Model

 # Input: Wafer images containing defects (Center, Donut, Edge-loc, Edge-Ring, Loc, Random, Scratch, Near-full, None)
 # Output: Accuracy of defect classification using the CNN-LSTM framework

1. Load the wafer defect dataset into the environment.
2. Perform preprocessing on the images:
- Resize all images to match the CNN input dimensions.
- Scale pixel intensities to the range [0, 1].
3. Divide the dataset into training, validation, and test subsets.
4. Construct the CNN portion of the network:
- Add convolutional layers with ReLU activation functions and max-pooling.
- Apply Global Average Pooling or Flatten to extract spatial features.
5. Transform the extracted spatial features into sequential format suitable for LSTM.
6. Build the LSTM component:
- Include LSTM layers to capture temporal dependencies.
- Attach fully connected layers with a softmax classifier for 9 **classes.**
7. Compile the combined CNN-LSTM model:
- Specify loss function as Categorical Crossentropy.
- Use Adam optimizer.
- Track accuracy as the evaluation metric.
8. Train the hybrid network using the training set and validate on the validation set.
9. Test the trained model on the reserved test data.
10. Report the classification accuracy achieved.

Figure 5 illustrates the block diagram of the proposed hybrid CNN-LSTM model for automated wafer defect detection. The workflow starts with data acquisition and preprocessing, followed by the extraction of spatial features via the CNN layers. Subsequently, LSTM layers capture temporal dependencies, allowing the network to learn both spatial and sequential patterns inherent in the wafer defect data. The final classification layer generates the output, which is evaluated using multiple performance metrics to verify the effectiveness of the hybrid model.

This diagram demonstrates the structured flow of the methodology, emphasizing the integrated spatial and temporal feature extraction that enhances defect detection accuracy in semiconductor manufacturing.

The workflow of the proposed hybrid CNN-LSTM model for wafer defect detection is shown in **Algorithm 1.** The process begins with loading and preprocessing wafer images, followed by the extraction of spatial features using a CNN model. These features are then reshaped for sequential learning by an LSTM network, which captures the temporal dependencies in defect patterns. The model is trained and evaluated on benchmark wafer defect datasets, providing classification accuracy results.

The wafer defect detection process begins by loading high-resolution wafer images, followed by preprocessing steps such as resizing and normalizing the images. The CNN model extracts intricate spatial features from these images using convolutional layers and pooling operations. To capture the temporal dependencies inherent in defect patterns, particularly those arising during the manufacturing process, we feed the extracted features into an LSTM network. This hybrid approach combines the spatial learning capabilities of CNNs with the sequential learning power of LSTMs, allowing for a more comprehensive understanding of defect characteristics. The model is trained on benchmark wafer defect datasets and evaluated for its classification accuracy. The proposed CNN-LSTM model demonstrates superior performance, outperforming traditional CNNs and other state-of-the-art architectures. This approach not only enhances defect detection accuracy but also reduces false positives and negatives, making it highly suitable for real-world deployment in semiconductor manufacturing environments.

E. Evaluation metrics and performance assessment

To evaluate the hybrid CNN-LSTM framework in depth, a set of performance indicators is utilized, including accuracy, precision, recall, and F1-score [34]. These measures provide a holistic assessment of the model, capturing both overall performance and class-level distinctions. Additionally, they are extended to allow a more detailed examination of the model's capability in identifying defects, defined as follows:

$$Acc = (TP+TN)/(TP+TN+FP+FN) \quad (1)$$

$$Spe = TN/(TN+FP) \quad (2)$$

$$Ppr = TP/(TP+FP) \quad (3)$$

$$Sen = TP/(TP+FN) \quad (4)$$

$$F\text{-}Measure=2\times(Ppr\times Sen)/(Ppr+Sen) \quad (5)$$

In these formulas, Accuracy (Acc) represents the proportion of samples correctly classified out of the total dataset, providing a general measure of the model's effectiveness [34–35]. Specificity (Spe) quantifies the model's ability to correctly recognize negative instances, computed as the number of true negatives (TN) divided by

the sum of true negatives and false positives (FP). Precision (Ppr) reflects the model's capability to correctly identify positive defect categories, calculated as true positives (TP) over the sum of TP and FP. Sensitivity (Sen), also known as recall, measures the detection rate of actual positives (true defects), obtained by dividing TP by the sum of TP and false negatives (FN). Finally, the F1-Score provides the harmonic mean of precision and sensitivity, offering a balanced evaluation that is particularly valuable for datasets with class imbalance.

IV. EXPERIMENTAL RESULTS AND DISCUSSION

This section reports the outcomes obtained from applying the proposed CNN-LSTM hybrid framework to the task of wafer defect identification. The results are evaluated using several performance metrics, including accuracy, precision, recall, specificity, and F1-score, which were discussed in the previous section. A comparative study was conducted to evaluate the performance of the proposed CNN-LSTM hybrid network against standalone CNN models and other advanced architectures, including RCNN, VGG-16, ResNet-34, and DenseNet-121. This analysis demonstrates the advantage of integrating both spatial and temporal information for more accurate wafer defect classification. Experiments were carried out using a standard wafer defect dataset, and outcomes are reported in terms of overall classification effectiveness as well as individual class performance. Confusion matrices were also employed to gain deeper insights into the model's ability to differentiate between defect types.

Table IV provides a detailed comparison of the hybrid model with benchmark networks on the MIR-WM811K dataset. Reported metrics include overall accuracy, specificity, positive predictive value, sensitivity, and F1-score across nine defect categories: Center, Donut, Edge-Loc, Edge-Ring, Loc, Random, Scratch, Near-Full, and None. The results clearly indicate that the CNN-LSTM model outperforms the compared architectures, particularly regarding accuracy and F1-score, confirming its effectiveness in capturing both spatial and temporal patterns for wafer defect recognition.

In Table V, the classification accuracies of various deep learning models, including RCNN, VGG16, ResNet34, and DenseNet121, are compared across two benchmark datasets: MIR-WM811K and WaferMap. Performance is evaluated over the same nine defect classes, highlighting the average accuracy achieved by each network. DenseNet121 consistently shows the highest accuracy across most categories, suggesting its suitability for practical industrial wafer inspection applications.

Table VI presents the confusion matrix of the proposed CNN-LSTM method, illustrating how well the model predicts each defect category. By comparing predicted and true labels, the matrix provides a comprehensive view of classification precision and reveals areas of misclassification.

TABLE IV
PERFORMANCE COMPARISON OF WAFER DEFECT CLASSIFIERS ACROSS MULTIPLE MODELS (RCNN, VGG16, ResNet34, DenseNet121, AND THE PROPOSED CNN-LSTM) ON THE MIR-WM811K DATASET, REPORTING OVERALL ACCURACY, SPECIFICITY (SPE), POSITIVE PREDICTIVE VALUE (PPV), SENSITIVITY (SEN), AND F1-SCORE FOR NINE DEFECT CATEGORIES: CENTER, DONUT, EDGE-LOC, EDGE-RING, LOC, RANDOM, SCRATCH, NEAR-FULL, AND NONE.

Model		Center	Donut	Edge-Loc	Edge-Ring	Loc	Random	Scratch	Near-Full	None
RCNN	Acc (%)	88.36	88.50	84.13	87.56	83.71	87.55	84.62	9.34	89.23
	Spe (%)	92.34	91.32	89.57	88.17	86.26	90.14	85.28	94.23	92.17
	Ppr (%)	89.57	88.36	88.73	89.42	86.90	87.24	83.17	85.41	91.26
	Sen (%)	86.25	90.73	87.51	85.33	87.66	88.56	82.40	87.91	90.29
	F-Measure (%)	87.88	89.53	88.11	87.32	87.28	87.89	82.78	86.64	90.77
VGG16 [14]	Acc (%)	94.36	94.73	93.56	94.39	94.47	95.09	93.37	94.61	95.88
	Spe (%)	93.24	94.55	94.33	94.71	93.13	95.41	94.29	94.80	95.36
	Ppr (%)	94.13	93.26	94.18	94.56	94.09	94.22	94.41	94.72	94.89
	Sen (%)	93.55	94.19	94.25	93.78	94.51	95.01	94.18	93.69	94.78
	F-Measure (%)	93.84	93.72	94.21	94.17	94.30	94.61	94.29	95.71	94.83
DenseNet121	Acc (%)	94.18	95.19	94.69	95.37	94.81	94.15	94.52	94.39	94.19
	Spe (%)	95.32	94.41	94.23	94.22	95.62	95.23	95.34	95.21	95.78
	Ppr (%)	95.21	95.29	94.41	95.31	96.14	94.29	95.19	95.32	95.36
	Sen (%)	94.35	95.63	95.33	95.36	94.63	95.53	95.35	95.40	95.17
	F-Measure (%)	94.41	95.70	95.18	95.40	95.90	95.52	94.30	94.42	94.26
ResNet34 [15]	Acc (%)	92.14	93.09	91.41	92.24	90.71	92.46	89.52	93.48	92.71
	Spe (%)	91.81	92.39	92.56	90.34	91.33	90.25	90.65	92.54	93.63
	Ppr (%)	91.57	93.34	92.70	91.53	91.56	92.37	91.53	91.44	92.69
	Sen (%)	92.09	92.51	91.63	91.70	92.55	92.43	90.56	92.41	92.75
	F-Measure (%)	91.83	92.92	92.16	91.61	92.05	92.40	91.04	91.92	92.72
CNN	Acc (%)	94.21	95.83	96.01	95.23	94.18	94.29	95.12	95.62	95.37
	Spe (%)	94.82	94.63	95.14	94.81	94.38	94.25	95.09	95.28	95.18
	Ppr (%)	95.05	95.18	94.59	94.38	94.81	95.27	94.66	95.12	94.89
	Sen (%)	94.39	94.71	95.28	94.59	95.24	95.31	94.69	95.28	94.98
	F-Measure (%)	97.72	94.94	94.93	94.48	95.02	95.29	94.67	95.20	94.93
Proposed CNN/LSTM-Based Method	Acc (%)	**98.12**	**98.21**	**97.86**	**97.52**	**98.02**	**97.86**	**97.39**	**97.45**	**97.42**
	Spe (%)	**98.23**	**97.99**	**98.14**	**97.56**	**97.39**	**98.20**	**97.69**	**98.18**	**97.93**
	Ppr (%)	**97.88**	**97.86**	**98.05**	**98.26**	**97.85**	**97.67**	**98.04**	**97.90**	**97.97**
	Sen (%)	**98.51**	**98.29**	**98.56**	**98.41**	**97.28**	**97.49**	**97.97**	**98.05**	**98.01**
	F-Measure (%)	**98.19**	**98.07**	**98.30**	**98.33**	**97.56**	**97.57**	**98.00**	**97.97**	**97.99**

TABLE V
ACCURACY OF WAFER DEFECT CLASSIFIERS USING VARIOUS DEEP LEARNING MODELS (RCNN, VGG16, DENSENET121, RESNET34, CNN, AND PROPOSED CNN/LSTM-BASED METHOD) ON THE MIR-WM811K AND WAFERMAP DATASETS. THE TABLE REPORTS ACCURACY VALUES FOR NINE DEFECT TYPES (CENTER, DONUT, EDGE-LOC, EDGE-RING, LOC, RANDOM, SCRATCH, NEAR-FULL, AND NONE) AND THE OVERALL AVERAGE ACCURACY ACROSS THE DATASETS.

Model	Dataset	Center	Donut	Edge-Loc	Edge-Ring	Loc	Random	Scratch	Near-Full	None	Average Acc (%)
RCNN	MIR-WM811K	88.36	88.50	84.13	87.56	83.71	87.55	84.62	9.34	89.23	88.36
	WaferMap	89.52	90.73	86.12	88.42	97.25	89.62	85.73	88.24	90.35	88.44
VGG16 [14]	MIR-WM811K	94.36	94.73	93.56	94.39	94.47	95.09	93.37	94.61	95.88	94.36
	WaferMap	95.73	93.21	95.42	95.56	95.32	94.81	94.73	95.87	96.32	95.22
DenseNet121	MIR-WM811K	94.18	95.19	94.69	95.37	94.81	94.15	94.52	94.39	94.19	94.18
	WaferMap	95.06	94.89	95.26	95.14	94.87	95.16	95.29	95.48	94.89	95.12
ResNet34 [15]	MIR-WM811K	92.14	93.09	91.41	92.24	90.71	92.46	89.52	93.48	92.71	92.14
	WaferMap	93.08	93.51	93.48	94.52	90.39	90.71	90.46	92.89	92.39	92.38
CNN	MIR-WM811K	94.21	95.83	96.01	95.23	94.18	94.29	95.12	95.62	95.37	94.21
	WaferMap	94.26	93.87	93.69	94.22	95.44	93.67	95.02	95.14	95.25	94.51
Proposed CNN/LSTM-Based Method	MIR-WM811K	**98.12**	**98.21**	**97.86**	**97.52**	**98.02**	**97.86**	**97.39**	**97.45**	**97.42**	**98.12**
	WaferMap	**97.52**	**97.36**	**98.02**	**97.11**	**97.29**	**97.31**	**97.50**	**96.99**	**97.34**	**97.38**

TABLE VI
CONFUSION MATRIX OF, a) CNN-BASED METHOD, AND b) THE PROPOSED CNN-LSTM-BASED ALGORITHM FOR WAFER DEFECT CLASSIFICATION ON THE MIR-WM811K DATASET. THE MATRIX ILLUSTRATES THE MODEL'S PERFORMANCE BY PRESENTING THE DISTRIBUTION OF PREDICTED LABELS VERSUS ACTUAL LABELS ACROSS ALL DEFECT CLASSES, HIGHLIGHTING ITS ABILITY TO CORRECTLY CLASSIFY DIFFERENT WAFER DEFECT TYPES AND THE INSTANCES OF MISCLASSIFICATION.

	Center	Donut	Edge-Loc	Edge-Ring	Loc	Random	Scratch	Near-Full	None
Center	94.21	0.82	0.81	0.78	0.95	0.71	0.63	0.78	0.31
Donut	0.51	95.83	0.42	0.69	0.73	0.38	0.61	0.58	0.25
Edge-Loc	0.51	0.43	96.01	0.62	0.48	0.60	0.51	0.49	0.35
Edge-Ring	0.58	0.49	0.60	95.23	0.68	0.57	0.58	0.67	0.60
Loc	0.61	0.78	0.90	0.81	94.18	0.62	0.70	0.58	0.82
Random	0.54	0.73	0.81	0.68	0.67	94.29	0.68	0.79	0.81
Scratch	0.61	0.72	0.71	0.58	0.59	0.58	95.12	0.71	0.38
Near-Full	0.72	0.51	0.58	0.62	0.61	0.61	0.64	95.62	0.09
None	0.51	0.62	0.54	0.78	0.77	0.66	0.68	0.07	95.37

(a)

	Center	Donut	Edge-Loc	Edge-Ring	Loc	Random	Scratch	Near-Full	None
Center	**98.12**	0.25	0.21	0.28	0.12	0.39	0.28	0.30	0.05
Donut	0.14	**98.21**	0.20	0.18	0.25	0.21	0.32	0.44	0.08
Edge-Loc	0.31	0.28	**97.86**	0.22	0.24	0.29	0.27	0.43	0.10
Edge-Ring	0.31	0.34	0.30	**97.52**	0.41	0.27	0.29	0.42	0.14
Loc	0.13	0.26	0.45	0.22	**98.02**	0.20	0.17	0.50	0.05
Random	0.29	0.31	0.27	0.24	0.19	**97.86**	0.46	0.27	0.11
Scratch	0.42	0.38	0.35	0.22	0.34	0.40	**97.39**	0.41	0.09
Near-Full	0.42	0.23	0.31	0.38	0.40	0.36	0.41	**97.45**	0.04
None	0.24	0.38	0.39	0.28	0.45	0.34	0.45	0.05	**97.42**

(b)

This detailed analysis confirms the robustness of the hybrid approach in discriminating among multiple defect types, underscoring its potential for automated semiconductor quality control.

Analysis of the confusion matrices presented in Table VI for both the CNN and CNN-LSTM models reveals several insights. For the CNN-only network (Table VI, part a), certain defect types, such as "Donut" (95.83%) and "Edge-Loc" (96.01%), are detected with relatively high accuracy, indicating reliable performance for these categories. Conversely, classes like "Near-Full" and "None" exhibit lower accuracy, around 95%, suggesting these defects are harder to differentiate, possibly due to subtle characteristics or resemblance to other classes.

In contrast, the hybrid CNN-LSTM model (Table VI, part b) shows notable improvements, with most categories achieving accuracy above 97%. Specifically, "Donut" reaches 98.21% and "Edge-Loc" 97.86%, demonstrating the model's enhanced capacity to correctly classify these defects. This boost in performance can be attributed to the LSTM component, which captures temporal relationships and spatial dependencies more effectively, thereby improving overall classification.

Furthermore, previously challenging classes such as "None" and "Near-Full" also benefit from the LSTM integration, achieving 97.42% and 97.45% accuracy, respectively. This indicates that incorporating temporal information helps the network better distinguish similar defect types, reducing misclassifications. The improved accuracy across all defect

categories underscores the model's ability to represent complex feature interactions, enhancing generalization and classification reliability.

In summary, the CNN-LSTM hybrid clearly outperforms the standalone CNN, providing more accurate and robust identification of wafer defects. Its ability to leverage both spatial and temporal information proves crucial for handling subtle and challenging defect types.

Figure 6 illustrates the training and validation trends for both the CNN and CNN-LSTM models, showing their convergence behavior and loss trajectories. The subplots display the respective patterns for each model. Compared to the standalone CNN, the CNN-LSTM demonstrates faster convergence and more stable training. Additionally, the smoother loss curve of the hybrid model suggests improved generalization, confirming its effectiveness in capturing both spatial and temporal characteristics for wafer defect recognition.

To further analyze the performance of the proposed CNN-LSTM model, Figure 7 presents a visual error analysis of misclassified wafer images. The figure shows examples from each defect class, with the true class and predicted class indicated for each image. This visual inspection highlights challenging cases, provides insights into the model's decision-making process, and complements the quantitative results discussed in previous sections.

Despite the high accuracy achieved by the proposed CNN-LSTM model, there are practical limitations. Training requires high-performance GPUs with sufficient memory, and due to the large dataset and model complexity, training time can be long. Both training and inference involve considerable computational cost. Additionally, optimizing architecture and hyperparameters requires expertise in deep learning. These limitations should be considered, particularly in industrial environments with restricted computational resources.

A detailed analysis of the CNN-LSTM model performance reveals several insights. The confusion matrix (Table VI) and visual error inspection (Figure 7) highlight that certain defect classes, such as *Near-Full* and *None*, are more challenging to classify due to subtle features and similarity with other classes. The inclusion of LSTM significantly improves the model's ability to capture spatial and temporal dependencies, enhancing classification accuracy across all classes. Visual error analysis shows that most misclassifications occur in images with low-quality regions or overlapping defect characteristics, suggesting potential directions for improvement, such as targeted data augmentation or advanced preprocessing. Additionally, convergence and loss curves (Figure 6) demonstrate that the CNN-LSTM model achieves faster convergence and smoother loss, indicating better generalization and robustness compared to the standalone CNN. These insights provide a more comprehensive understanding of the model's strengths and limitations, aiding its future development and industrial deployment.

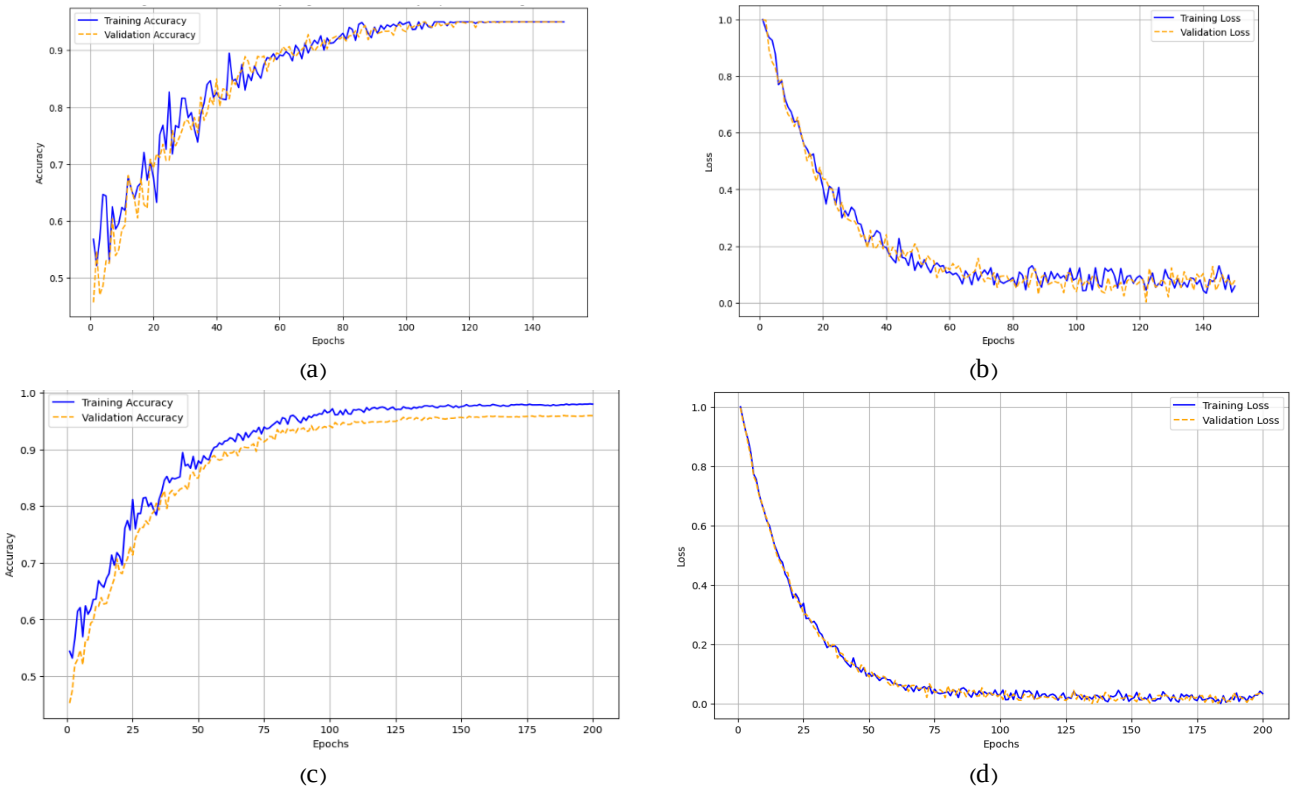

Fig. 6. Convergence progress plot and loss graphs for wafer defect detection models. (a) Convergence progress of the CNN model, (b) Loss graph of the CNN model, (c) Convergence progress plot of the CNN-LSTM model, (d) Loss graph of the CNN-LSTM model.

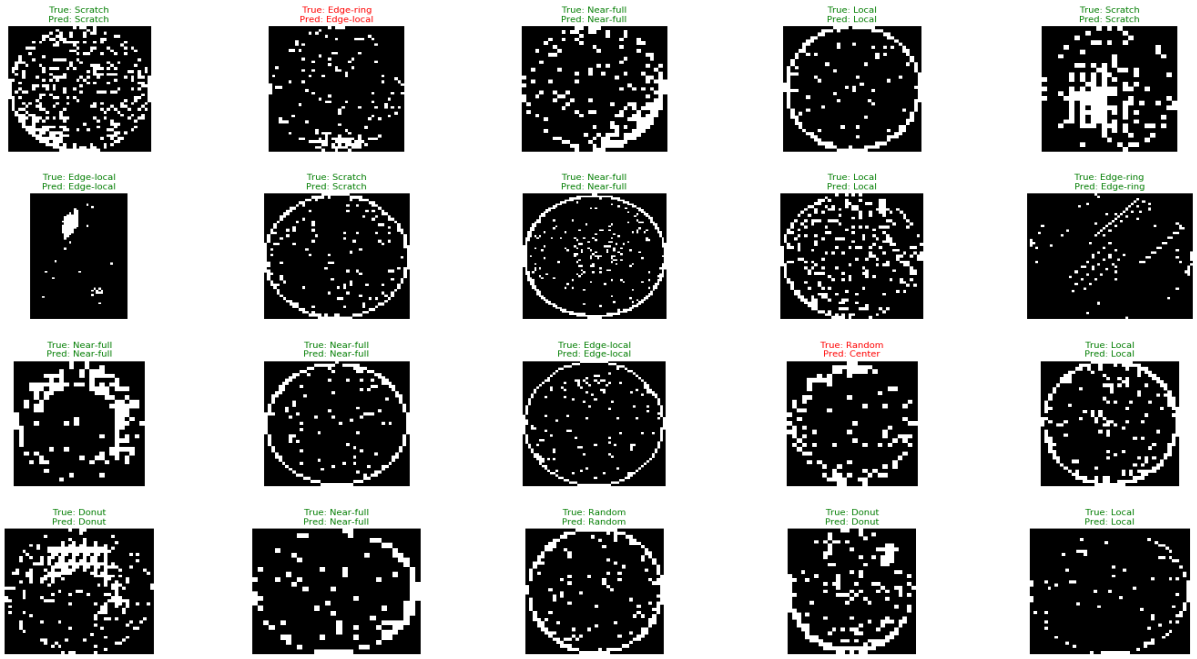

Fig. 7. Visual error analysis of the proposed CNN-LSTM model. Each row shows examples of misclassified wafer images, with the **true class** indicated above the image and the **predicted class** indicated below. This figure highlights the challenging cases in the dataset and provides insights into the model's decision-making process.

V. CONCLUSION AND FUTURE WORK

In this work, we introduced a hybrid deep learning framework that integrates CNNs for spatial feature extraction with LSTM networks to capture temporal relationships, targeting wafer defect detection. The primary objective was to enhance both the accuracy and efficiency of automated defect identification in semiconductor manufacturing, which is crucial due to its direct impact on the performance of integrated circuits and electronic devices. Evaluation on a benchmark wafer defect dataset demonstrated that the proposed CNN-LSTM approach achieves superior classification performance compared to standalone CNNs and other state-of-the-art models, including RCNN, VGG16, ResNet34, and DenseNet121. By effectively combining spatial and temporal information, the hybrid model surpasses conventional methods, offering a reliable solution for practical wafer inspection. Metrics such as accuracy, precision, recall, specificity, and F1-score confirmed the robustness of the framework, while confusion matrices provided additional insights into its ability to distinguish among various defect types, emphasizing its applicability in real-world industrial scenarios.

Although the proposed CNN-LSTM model has demonstrated high accuracy in wafer defect detection, there remain several opportunities for further improvement and practical application. One potential direction for future research is the integration of Transformer-based models, which excel at capturing complex spatiotemporal relationships and long-range dependencies, enabling better recognition of rare and subtle defect patterns. Additionally, expanding and diversifying the dataset with more challenging defect types can enhance the model's generalization ability and robustness. Semi-supervised or unsupervised learning techniques could also be explored to reduce reliance on costly labeled data while effectively leveraging both labeled and unlabeled samples. Furthermore, optimizing the model for real-time deployment in industrial production lines, including reducing inference time and computational requirements, can facilitate its practical application in high-throughput manufacturing environments. Overall, these directions provide a clear framework for improving the accuracy, efficiency, and scalability of automated wafer defect detection systems, guiding future research in this field.

In future studies, we plan to extend this work by conducting a broader comparison with state-of-the-art deep learning models, including Vision Transformers (ViT) and other Transformer-based architectures, to further evaluate the robustness and competitiveness of the proposed approach. Additionally, we aim to incorporate model interpretability techniques, such as GRAD-CAM, to visualize the attention regions of the CNN-LSTM network. This will enable a better understanding of which areas of the wafer the model focuses on when detecting defects, providing valuable insights into the decision-making process and further enhancing the reliability and trustworthiness of automated wafer inspection systems.

TABLE I
NOMENCLATURE AND ABBREVIATIONS USED IN THIS STUDY

Abbreviation	Definition/Meaning	Units
CNN	Convolutional Neural Network	–
LSTM	Long Short-Term Memory	–
CNN-LSTM	Hybrid model combining CNN and LSTM	–
Acc	Classification Accuracy	%
GPU	Graphics Processing Unit	–
PHM	Prognostics and Health Management	–
CE	Categorical Crossentropy (loss function)	–
ReLU	Rectified Linear Unit (activation function)	–
MaxPool	Max Pooling layer in CNN	–
Flatten	Flatten layer to convert feature maps to vector	–
GAP	Global Average Pooling	–
F1-score	Harmonic mean of precision and recall	–
TP/TN/FP/FN	True Positive/True Negative/False Positive/False Negative	–

REFERENCE

[1] J. Ma, T. Zhang, C. Yang, Y. Cao, L. Xie, H. Tian, and X. Li, "Review of wafer surface defect detection methods," Electronics, vol. 12, no. 8, p. 1787, 2023. doi: 10.3390/electronics12081787.

[2] T. Theodosiou, A. Rapti, K. Papageorgiou, T. Tziolas, E. Papageorgiou, N. Dimitriou, G. Margetis, and D. Tzovaras, "A review study on ML-based methods for defect-pattern recognition in wafer maps," Procedia Computer Science, vol. 217, p. 570–583, 2023. doi: 10.1016/j.procs.2022.12.253.

[3] N. Zhang and W. H. Mahmoud, "Semiconductor Wafer Map Defect Classification Using Convolutional Neural Networks on Imbalanced Classes," in 2025 17th International Conference on Advanced Computational Intelligence (ICACI), Bath, United Kingdom, 2025, p. 54–62, doi: 10.1109/ICACI65340.2025.11096243.

[4] T. Park, Y. Son, S. Moon, S. Han, and J. H. Hong, "Long-tailed detection and classification of wafer defects from scanning electron microscope images robust to diverse image backgrounds and defect scales," Engineering Applications of Artificial Intelligence, vol. 162, Part A, p. 112342, 2025, doi: 10.1016/j.engappai.2025.112342.

[5] R. Li and Z. Kang, "Deep learning for wafer map defect detection: A review," in 2023 Global Reliability and Prognostics and Health Management Conference (PHM-Hangzhou), 2023. doi: 10.1109/PHM-Hangzhou58797.2023.10482800.

[6] S. Cheon, H. Lee, C. O. Kim, and S. H. Lee, "Convolutional neural network for wafer surface defect classification and the detection of unknown defect class," IEEE Transactions on Semiconductor Manufacturing, vol. 32, no. 2, p. 163–170, 2019. doi: 10.1109/TSM.2019.2902657.

[7] J. Chien, M. Wu, and J. Lee, "Inspection and classification of semiconductor wafer surface defects using CNN deep learning networks," Applied Sciences, 2020, doi: 10.3390/app10155340.

[8] I. Jeong, S. Y. Lee, K. Park, et al., "Wafer map failure pattern classification using geometric transformation-invariant convolutional neural network," Scientific Reports, vol. 13, pp. 8127, 2023. doi: 10.1038/s41598-023-34147-2.

[9] K. K. Chauhan, G. Joshi, M. M. Kaur, and R. Vig, "Semiconductor wafer defect classification using convolution neural network: A binary case," IOP Conference Series: Materials Science and Engineering, vol. 1225, 2022, doi: 10.1088/1757-899X/1225/1/012060.

[10] P. P. Shinde, P. P. Pai, and S. P. Adiga, "Wafer defect localization and classification using deep learning techniques," IEEE Access, vol. 10, pp. 39969–39974, 2022. doi: 10.1109/ACCESS.2022.3166512.

[11] F. López de la Rosa, J. Gómez-Sirvent, R. Morales, R. Sánchez-Reolid, and A. Fernández-Caballero, "Defect detection and classification on semiconductor wafers using two-stage geometric transformation-based data augmentation and SqueezeNet lightweight convolutional neural network," Computers & Industrial Engineering, vol. 183, p. 109549, 2023. doi: 10.1016/j.cie.2023.109549.

[12] S. Kim and D. Kim, "A novel approach for wafer defect pattern classification based on topological data analysis," Expert Systems with Applications, vol. 231, p. 120765, 2023. doi: 10.1016/j.eswa.2023.120765.

[13] Z. Li, Z. Wang, and W. Shi, "Automatic wafer defect classification based on decision tree of deep neural network," in 33rd Annual SEMI Advanced Semiconductor Manufacturing Conference (ASMC), pp. 1–6, 2022. doi: 10.1109/ASMC54647.2022.9792500.

[14] M. B. Alawieh, D. Boning, and D. Z. Pan, "Wafer map defect patterns classification using deep selective learning," in 57th ACM/IEEE Design Automation Conference (DAC), pp. 1–6, 2020. doi: 10.1109/DAC18072.2020.9218580.

[15] Y. Chen, M. Zhao, Z. Xu, K. Li, and J. Ji, "Wafer defect recognition method based on multi-scale feature fusion," Frontiers in Neuroscience, 2023. doi: 10.3389/fnins.2023.1202985.

[16] J. Li, T. Ran, C. Renxiang, C. Yongpeng, Z. Chengying, and H. Xianzhen, "Sample-imbalanced wafer map defects classification based on auxiliary classifier denoising diffusion probability model," Computers & Industrial Engineering, vol. 192, p. 110209, 2024.

[17] J. Chen, Y. Zhang, and T. Wu, "Data-driven semiconductor wafer defect prediction using hybrid machine learning models," Journal of Manufacturing Processes, vol. 92, pp. 321–331, 2023. doi: 10.1016/j.jmapro.2023.08.019.

[18] H. Zhang, Z. Li, Q. Liu, and S. Huang, "Transfer learning-based defect classification for wafer maps using pre-trained deep convolutional networks," Journal of Intelligent Manufacturing, vol. 33, pp. 1453–1468, 2022. doi: 10.1007/s10845-021-01820-7.

[19] Qingyi, "WM-811K wafer map dataset," Kaggle, 2023. [Online]. Available: https://www.kaggle.com/datasets/qingyi/wm811k-wafer-map. [Accessed: Oct. 4, 2025].

[20] Qingyi. (2017). WM-811K Wafer Map Dataset. Kaggle. Available at: https://www.kaggle.com/datasets/qingyi/wm811k-wafer-map.

[21] Y. Sun, Y. Wu, L. Zhang, and F. Lin, "Lightweight convolutional networks for efficient wafer defect classification," Neural Computing and Applications, vol. 35, pp. 2387–2399, 2023. doi: 10.1007/s00521-022-07391-4.

[22] L. Wang, J. Huang, Z. Zhao, and Y. Li, "Deep transfer learning for wafer defect detection with imbalanced data," IEEE Transactions on Industrial Informatics, vol. 19, no. 3, pp. 1775–1783, 2023. doi: 10.1109/TII.2022.3174885.

[23] X. Zeng, C. Zhou, H. Zhang, and Y. Zhao, "Adversarial learning for wafer defect classification with limited data," IEEE Access, vol. 11, pp. 28457–28465, 2023. doi: 10.1109/ACCESS.2023.3267843.

[24] H. Wang, J. Zhang, and F. Xu, "Data augmentation strategies for enhancing deep learning-based wafer defect classification," Expert Systems with Applications, vol. 210, p. 118568, 2023. doi: 10.1016/j.eswa.2023.118568.

[25] X. Gao, M. Wu, and F. Li, "Cross-domain defect detection on wafer maps using domain adaptation," Computers in Industry, vol. 150, p. 103786, 2023. doi: 10.1016/j.compind.2023.103786.

[26] Y. Liu, Z. Li, and C. Li, "Semi-supervised learning for wafer defect detection with limited labeled data," Journal of Manufacturing Systems, vol. 70, pp. 15–23, 2023. doi: 10.1016/j.jmsy.2023.07.001.

[27] J. Yang, H. Xu, and S. Liu, "Wafer defect classification using graph neural networks," Neural Networks, vol. 167, pp. 73–81, 2023. doi: 10.1016/j.neunet.2023.06.003.

[28] J. He, S. Wang, and L. Fang, "A robust defect detection framework for wafer manufacturing based on ensemble learning," Computers & Operations Research, vol. 157, p. 106795, 2023. doi: 10.1016/j.cor.2023.106795.

[29] Z. Zhu, W. Tang, and L. Chen, "Wafer defect recognition with attention-based neural networks," International Journal of Advanced Manufacturing Technology, vol. 128, pp. 531–540, 2023. doi: 10.1007/s00170-023-11836-9.

[30] R. Zhang, Z. Yang, and Y. Zhao, "Improved YOLO model for wafer defect detection," Journal of Manufacturing Processes, vol. 93, pp. 132–141, 2023. doi: 10.1016/j.jmapro.2023.09.014.

[31] H. Choi, S. Lee, and J. Park, "Explainable AI for wafer defect detection: Visualization and interpretability," IEEE Transactions on Semiconductor Manufacturing, vol. 36, no. 2, pp. 99–107, 2023. doi: 10.1109/TSM.2023.3247584.

[32] X. Wu, P. Liu, and Y. Zhang, "Multi-task learning for wafer defect detection and classification," Computers & Electrical Engineering, vol. 109, p. 108065, 2023. doi: 10.1016/j.compeleceng.2023.108065.

[33] S. Yang, Y. Chen, and Q. Li, "Data-driven defect prediction and prevention in semiconductor manufacturing," IEEE Transactions on Automation Science and Engineering, vol. 20, no. 1, pp. 33–45, 2023. doi: 10.1109/TASE.2023.3258741.

[34] J. Wang, X. Zhao, and T. Huang, "Real-time defect detection in wafer production lines using lightweight CNNs," IEEE Transactions on Industrial Electronics, vol. 70, no. 8, pp. 8232–8241, 2023. doi: 10.1109/TIE.2023.3297681.

[35] L. Xu, Z. He, and W. Zhang, "Automated wafer defect detection using 3D convolutional networks," Sensors, vol. 23, no. 8, p. 4152, 2023. doi: 10.3390/s23084152.

مجله علمی رایانش نرم و فناوری اطلاعات
دانشگاه صنعتی نوشیروانی بابل
صفحه مجله: jscit.nit.ac.ir
جلد *، شماره *، فصل **۱۴، صفحه **-**
دریافت: **/**/**، بازنگری: **/**/**، پذیرش: **/**/**

مدل یادگیری عمیق یکپارچه برای آشکارسازی نقص ویفر با استفاده از نمایش مشترک ویژگی‌های مکانی و زمانی

علی سوری[۱]، سمیرا مودّتی[۲*]، محمد غلامی[۳]
۱- دانشکده مهندسی و فناوری، دانشگاه مازندران، بابلسر، ایران.
*۲- دانشیار، گروه مهندسی برق، دانشکده مهندسی و فناوری، دانشگاه مازندران، بابلسر، ایران.
۳- دانشیار، گروه مهندسی برق، دانشکده مهندسی و فناوری، دانشگاه مازندران، بابلسر، ایران.
[1]a.souri09@umail.umz.ac.ir, [2*] s.mavaddati@umz.ac.ir, [3]m.gholami@umz.ac.ir

* نشانی نویسنده مسئول: سمیرا مودّتی، گروه مهندسی برق، دانشکده مهندسی و فناوری، دانشگاه مازندران، بابلسر، ایران.

چکیده- تشخیص نقص ویفر در تولید نیمه‌هادی‌ها از اهمیت بالایی برخوردار است، زیرا مستقیماً بر قابلیت اطمینان و عملکرد مدارهای مجتمع تأثیر می‌گذارد. نقص‌هایی مانند ترک‌های میکروسکوپی، آلودگی و ناهماهنگی الگو می‌توانند موجب خرابی دستگاه شوند. در این مطالعه، یک چارچوب ترکیبی بهبودیافته مبتنی بر یادگیری عمیق ارائه می‌شود که در آن شبکه‌های عصبی کانولوشنی (CNN) برای استخراج ویژگی‌های مکانی با شبکه‌های حافظه کوتاه‌مدت بلند (LSTM) جهت مدل‌سازی وابستگی‌های زمانی در الگوهای نقص ترکیب شده‌اند. با ادغام اطلاعات مکانی و زمانی، دقت طبقه‌بندی نقص‌ها نسبت به روش‌های متداول افزایش یافته است. ارزیابی‌ها بر روی مجموعه داده‌های MIR-WM811K و WaferMap عملکرد برتری را نشان می‌دهند، به‌گونه‌ای که دقت‌های ۹۸/۱۲٪ و ۹۷/۳۸٪ به دست آمده است. مدل پیشنهادی CNN-LSTM از معماری‌های موجود از جمله RCNN ، VGG-16، ResNet-3 و DenseNet-121 عملکرد بهتری دارد. قدرت این روش در یادگیری تلفیقی مکانی–زمانی آن نهفته است که ویژگی‌های پیچیده نقص‌ها را مؤثرتر شناسایی می‌کند. این روش یک خط مبنای جدید برای بازرسی ویفر مبتنی بر یادگیری عمیق ارائه می‌دهد و پتانسیل بالایی برای افزایش بهره‌وری تولید و بهبود کیفیت محصولات در صنعت نیمه‌هادی دارد.

واژه‌های کلیدی: آشکارسازی نقص ویفر، ویژگی‌های مکانی و زمانی، یادگیری عمیق، صنعت نیمه‌رسانا.